A Schur-Complement Model-Order-Reduction Technique for the Finite Element Solution of Transient Elastohydrodynamic Lubrication Problems

W. Habchi*

Lebanese American University, Department of Industrial and Mechanical Engineering, Byblos, Lebanon

*Corresponding author: wassim.habchi@lau.edu.lb

Abstract

The current work presents reduced order finite element modeling framework for the solution of transient elastohydrodynamic lubrication (EHL) problems. The model order reduction technique is based on a Schur-complement method, applied to the elastic part within EHL problems. As such, it is exact and introduces no additional errors to the solution, with respect to the standard non-reduced finite element model. The technique reduces by one, the dimension of the linear elasticity part within the EHL problem. The use of the Schur-complement method however leads to a semi-dense Jacobian matrix. This is why the technique is complemented with a splitting procedure, allowing it to retrieve a standard finite-element-like sparsity pattern. In terms of computational performance, it is shown through a set of numerical experiments that the proposed reduced model offers a speed-up in computational times of the order of 15:1, compared to the equivalent full model, without any compromise on the accuracy of the solution.

Keywords: Transient Elastohydrodynamic Lubrication; Finite Elements; Model Order Reduction; Schur-Complement Method.

1. Introduction

Elastohydrodynamic lubrication (EHL) is a full film lubrication regime, encountered in lubricated machine elements in relative motion (e.g. roller element bearings, gears, cam-followers, etc.), whereby contacting surfaces are fully separated by a lubricant film. The particularity of this regime is that hydrodynamic pressures generated within the lubricating film are high enough to induce elastic displacement of the contacting solids. Thus, EHL problems are multi-physical in nature, involving a strong coupling between hydrodynamics (governing lubricant flow through the contact) and linear elasticity (governing the elastic displacement of the contacting solids); assuming isothermal conditions. Under thermal conditions, heat transfer (within the lubricant film and bounding solids) adds up to the list of coupled physics. An additional layer of complexity stems from the dependence of lubricant properties (e.g. density, viscosity, etc.) on contact parameters (e.g. pressure, temperature, shear stress, etc.) which makes the EHL problem strongly nonlinear. This being said, numerical solutions of EHL problems are often difficult to reach and require highly specialized modeling techniques.

As a clear testimony to the complexity of the EHL problem resolution, over the years, numerous modeling approaches were developed. Probably, the most widely used one to date is the so-called “multigrid” approach [1]. It is based on a weakly-coupled resolution of the governing equations and uses a finite difference discretization of the hydrodynamic part of the problem (Reynolds [2] equation). A multigrid resolution is employed to speed-up convergence. As for the linear elasticity part, a semi-analytical half-space approach [3] is employed. It consists of an integral evaluation over the entire contact domain, to estimate the surface elastic displacement at each point of the contact. Multigrid techniques are also employed to speed-up the integral evaluations. The use of a half-space approach though, for the linear elasticity part of the problem, prevents the establishment of a full-coupling with other physics. This is because the corresponding integral evaluations have to be carried out separately, from a knowledge of the hydrodynamic pressure field, determined from the solution of Reynolds equation.

In recent years, a finite element modeling (FEM) framework was introduced by the author and his co-workers [4] [5], allowing a fully-coupled resolution of the EHL problem, using a Newton-like method. In this framework, the elastic part of the EHL problem is based on a resolution of the classical linear elasticity equations, which can be fully-coupled to the solution of other governing equations. The downside however, is an extension of the elastic problem to the subsurface of the contacting solids. This extension is often unnecessary (except in some special cases e.g. rolling contact fatigue damage evaluation [6]) for the solution of the EHL problem, which only requires determining surface displacements, for the sake of defining the geometry of the lubricating gap. Nonetheless, the use of a finite element discretization, which enables the use of non-regular non-structured meshing, along with the use of higher-order elements in discretizing the hydrodynamic pressure field, kept the size of the model (number of unknowns) at an acceptable level. Besides, given the fast convergence characteristics of fully-coupled resolution schemes and Newton methods, this approach was found to be at least as competitive as state-of-the-art ones in terms of computational performance. Yet, a major improvement to these models was still possible, through the use of Model Order Reduction (MOR) techniques [7].

The last few years witnessed an emergence of application of MOR techniques to the aforementioned FEM treatment of EHL problems. First, Habchi et al. [8] [9] applied an EHL-specific component-mode-synthesis-like technique to the linear elasticity part of the EHL problem, reducing it to less than 30 degrees of freedom / unknowns. Later, Krinner and Rixen [10] introduced similar MOR techniques to reduce the size of the linear elasticity part, using Craig-Bampton reduction methods [11]. Using a similar approach, Maier et al. [12] [13] extended the reduction process to the hydrodynamic part too, leading to an even higher reduction order and faster computational times. Given the high reduction order in all of the aforementioned reduction techniques, they offer an extremely fast resolution process that is hard to beat in terms of computational speed. However, they suffer from two shortcomings. First, they entail a rather complex offline phase, requiring a high level of expertise in the generation of the basis functions that form the reduced solution space. Second, their solution scheme suffers from a loss of

generality. This is because the reduced solution space is generated under a given set of assumptions and conditions (e.g. smooth surfaces, isothermal Newtonian conditions, etc.). Any change in these conditions or the incorporation of any new features would require the generation of a new reduced solution space to include these features and their influence on the solution. In a recent work, Habchi and Issa [14] presented a new MOR technique that alleviates the above shortcomings, but leads to a lower reduction order. It consists in applying to the linear elasticity part of the EHL problem a Schur-complement method [15], also known as static condensation, Guyan condensation, sub-structuring or also domain decomposition method. First, the Schur-complement method is based on simple concepts of linear algebra, accessible to novice users. Second, the method is exact, as it simply consists in eliminating / condensing out unwanted degrees of freedom, called “slaves”, by injecting their effect into the needed retained ones, called “masters”. This leads however to a semi-dense Jacobian matrix. This is why the technique was complemented with a splitting procedure that allows it to retrieve a standard finite-element-like sparsity pattern. The technique was dubbed “Static Condensation with Splitting” (SCS).

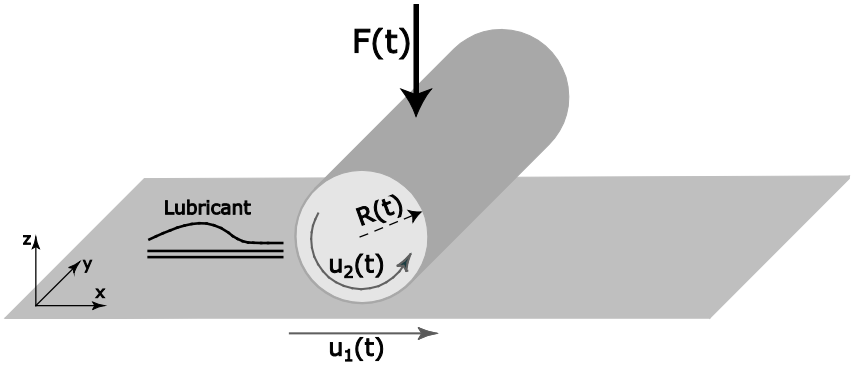

Figure 1: Equivalent geometry of a transient EHL line contact

All of the aforementioned MOR techniques were applied to EHL contacts operating under steady-state regime. However, in practice, EHL contacts are often subject to dynamic conditions e.g. variable external applied loads, surface speeds or even gap geometry. The current work extends the SCS technique, introduced in [14], to incorporate transient effects. Such an extension is not possible for any of the other MOR techniques mentioned above, without the need for repeating their offline phase, every time a new feature is considered. This can turn out to be prohibitive, as the computational cost associated with the offline phase of these MOR techniques often exceeds the cost of running their equivalent full models, which defies the purpose of reduced order modeling. The modeling framework proposed in this work can be applied to line or point contacts, operating under isothermal or thermal, Newtonian or non-Newtonian conditions. However, out of simplicity, only line contacts are considered, under isothermal Newtonian regime. Line contacts involve contacting elements that are infinitely long in one of the principal space directions, compared to other directions. In practice, this reduces by one the dimension of all parts of the EHL problem, since contact parameters (pressure, elastic displacement, etc.) do not vary in the infinitely long direction. Such contacts are encountered in spur gears or cylindrical roller element bearings for instance. The geometry of a line contact can

be reduced to an equivalent geometry; that of a contact between a rigid plane (denoted by the subscript 1) and an elastic cylinder of equivalent radius R (denoted by the subscript 2), moving at surface velocities u_1 and u_2, respectively, subject to an external applied load per unit length F. This is done by using appropriate equivalent solid material properties for the cylinder, as will be discussed in section 2. The equivalent geometry of a line contact is shown in Figure 1, whereby all contact parameters (i.e. surface velocities u_1 and u_2, cylinder radius R and external applied load per unit length F) may vary in time.

2. Governing Equations

In this section, the governing equations of the transient isothermal Newtonian EHL line contact problem and their associated boundary conditions are provided. All equations are written in dimensionless form, using Hertzian contact parameters [16] i.e. Hertzian contact half-width a_h and pressure p_h, defined as follows:

$$a_h = \sqrt{\frac{4FR}{\pi E}} \quad \text{and} \quad p_h = \frac{2F}{\pi a_h} \quad \text{with:} \quad E = \frac{1}{\frac{1-\upsilon_1^2}{E_1} + \frac{1-\upsilon_2^2}{E_2}} \tag{1}$$

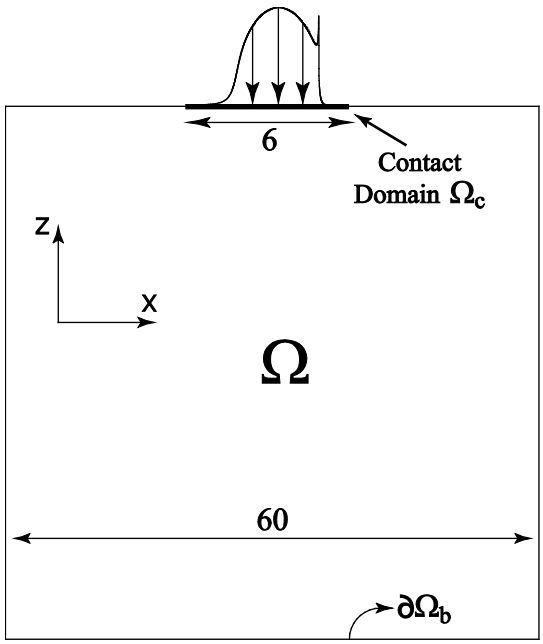

Figure 2: Computational domain of the transient EHL line contact problem

Note that E corresponds to the equivalent Young's modulus, defined as a function of the Young's moduli E_1 and E_2 of the two solids and their Poisson coefficients υ_1 and υ_2. It is used for the material of the elastic cylinder, along with an equivalent Poisson ratio $\upsilon = 0$ [5]. The use of equivalent material properties for the elastic cylinder (while assuming a rigid plane) allows it to accommodate the total elastic displacement of the two solids. This way, the linear elasticity equations are only applied to the domain representing the cylinder. The computational domain

for the transient EHL line contact problem is shown in Figure 2. Given the infinitely long nature of the contact in the *y*-direction, the solid computational domain is reduced to a two-dimensional one, in the *xz*-plane. It corresponds to a sufficiently large square domain Ω (to ensure a half-space configuration). Since thin-film assumptions imply no pressure variations within the film thickness (z-direction), the contact domain Ω_c is one-dimensional (in the *x*-direction) and it is located on the top side of Ω: $-4.5 \le X \le 1.5$, with the dimensionless space coordinates X and Z defined as: $X = x/a_h$ and $Z = z/a_h$. In order to ensure a half-space configuration, the square sides need to be at least 10 times larger than the size of the contact domain [4]. The dimensionless elastic displacement field $\bar{U} = \{U, W\}$ of the solids (where the x and z components U and W are defined as a function of their dimensional counterparts u and w as follows: $U = uR/a_h^2$ and $W = wR/a_h^2$), under the influence of the hydrodynamic pressure field p generated within the lubricant film, is obtained by applying plane strain linear elasticity equations to Ω, while applying a normal downward pressure force ($\sigma_n = -p$, where σ_n is the normal component of the stress tensor) over Ω_c and a zero displacement boundary condition over $\partial\Omega_b$. A free displacement boundary condition is applied to the remainder boundaries of Ω. Raisin et al. [17] showed that for EHL problems, the characteristic time scale for the elastic displacement of the solids is orders of magnitude smaller than other characteristic times of the problem. As such, the transient response of the solids may be neglected and these are assumed to deform instantaneously under any load variations. This being said, given the equivalent elastic material properties (E, υ) defined earlier, after simplification, the dimensionless plane strain elasticity equations and their associated boundary conditions reduce to:

$$
\begin{aligned}
&-\frac{\partial^2 U}{\partial X^2} - \frac{\partial}{\partial Z}\left[\frac{1}{2}\left(\frac{\partial U}{\partial Z} + \frac{\partial W}{\partial X}\right)\right] = 0 \\
&-\frac{\partial}{\partial X}\left[\frac{1}{2}\left(\frac{\partial U}{\partial Z} + \frac{\partial W}{\partial X}\right)\right] - \frac{\partial^2 W}{\partial Z^2} = 0
\end{aligned}
\qquad (2)
$$

$$
\text{Boundary Conditions:} \begin{cases} \dfrac{\partial W}{\partial Z} = -\dfrac{P}{2} \quad \text{and} \quad \sigma_t = 0 & \text{over } \Omega_c \\ U = W = 0 & \text{over } \partial\Omega_b \\ \sigma_n = \sigma_t = 0 & \text{elsewhere} \end{cases}
$$

In the above, σ_n and σ_t correspond to the normal and tangential components, respectively, of the stress tensor. Note that, the write-up of the linear elasticity equations and their associated boundary conditions provided in equation (2) is made independent of the solid material

properties (after simplification), through the use of dimensionless variables. A closer look at these equations reveals though that an indirect dependence on solid material properties exists. In fact, remember that the dimensionless displacement components U and W are defined as a function of the Hertzian contact half-width a_h and the dimensionless pressure P is defined as a function of the Hertzian pressure p_h. But both a_h and p_h depend on the solid material properties, as can be seen from their definitions provided in equation (1). The independence from solid material properties of the write-up of equation (2) is key to the model order reduction technique employed in the current work, as it would prevent repeating its offline phase every time any of the solid material properties is changed, as will be detailed in section 3.3.

The dimensionless hydrodynamic pressure $P = p/p_h$ generated over the contact domain is obtained by applying Reynolds [2] equation to Ω_c:

$$
\begin{gathered}
-\frac{\partial}{\partial X}\left(\bar{\varepsilon}\frac{\partial P}{\partial X}\right)+\frac{\partial\left(\bar{\rho}H\right)}{\partial X}+\frac{1}{\beta}\frac{\partial\left(\bar{\rho}H\right)}{\partial \bar{t}}+\underbrace{\xi\, P\,\Theta\left(-P\right)}_{\text{Penalty Term}}=0 \qquad \text{for} \quad t_0<\bar{t}\le\tilde{t} \\
\text{with}: \quad \bar{\varepsilon}=\frac{\bar{\rho}H^3}{\bar{\mu}\,\lambda} \quad \text{and} \quad \lambda=\frac{12\,u_m\,\mu_0\,R^2}{a_h^3\,p_h} \\
\text{Initial Conditions}: \quad P\left(X,t_0\right)=P_0\left(X\right) \quad \text{over } \Omega_c \\
\text{Boundary Conditions}: \begin{cases} P=0 & \text{at } X=-4.5 \quad \forall \bar{t} \\ P=0 & \text{at } X=1.5 \quad \forall \bar{t} \end{cases}
\end{gathered}
\tag{3}
$$

where $u_m=\left(u_1+u_2\right)/2$ is the mean entrainment speed of the contacting surfaces and β is a parameter that depends on the definition of the dimensionless time $\bar{t}$, which covers an interval spanning between an initial time t_0 and a final time $\tilde{t}$. In fact, depending on the application at hand, the definition of $\bar{t}$ as a function of its dimensional counterpart t may differ, resulting in a different expression for β. Therefore, at this point, the dimensionless time $\bar{t}$ will not be defined. Its definition and the resulting definition of the parameter β will be provided on a case-by-case basis, depending on the problem at hand (see section 4). Note that a penalty term has been added to Reynolds equation to force the non-physical negative pressures that arise in the solution towards zero [5]. In this term, Θ is simply the Heaviside function, while ξ is an arbitrary sufficiently large parameter. At this stage, the initial dimensionless pressure distribution $P_0\left(X\right)$ over the contact domain will not be specified as it is specific to the problem at hand. The dimensionless lubricant film thickness $H=hR/a_h^2$ (with h being its dimensional counterpart) appearing in Reynolds equation is defined over the contact domain Ω_c as:

$$
H\left(X,\bar{t}\right)=H_0\left(\bar{t}\right)+\frac{X^2}{2}-W\left(X,\bar{t}\right)+\bar{S}\left(X,\bar{t}\right) \tag{4}
$$

The first right-hand-side term in the above equation corresponds to the rigid body separation of the solids, while the second describes the non-deformed geometry of the lubricant gap. The third term represents the normal displacement of the solids within the contact domain, under the influence of the hydrodynamic pressure field. The last term allows for the incorporation of surface features into the description of the lubricant gap geometry. The pressure-dependence of the dimensionless lubricant density $\bar{\rho} = \rho/\rho_0$ and viscosity $\bar{\mu} = \mu/\mu_0$ (where ρ and μ are their dimensional counterparts, whose ambient pressure values are denoted by the subscript 0) within Reynolds equation are described by the Dowson and Higginson [18] and Roelands [19] relationships, respectively:

$$\bar{\rho} = 1 + \frac{0.6\times10^{-9} P\, p_h}{1+1.7\times10^{-9} P\, p_h}$$

$$\bar{\mu} = \exp\left\{\left(\ln\left(\mu_0\right)+9.67\right)\left[-1+\left(1+5.1\times10^{-9} P\, p_h\right)^{Z_0}\right]\right\} \tag{5}$$

$$\text{with:}\quad Z_0 = \frac{\alpha}{\left[5.1\times10^{-9}\left(\ln\left(\mu_0\right)+9.67\right)\right]}$$

Finally, the load balance equation is used to ensure equilibrium of forces within the contact, between the external applied load per unit length F and the hydrodynamic pressure field p, generated within the lubricant film, while neglecting inertia and body forces. In dimensionless form, it is given by:

$$\int_{\Omega_c} P\, dX = \frac{\pi}{2} \tag{6}$$

The load balance equation is added as a simple integral equation, to the system of equations formed by the linear elasticity and Reynolds equations, while introducing the rigid body separation term H_0 as an additional scalar unknown.

3. FEM Model description

The transient isothermal Newtonian EHL line contact problem is governed by the linear elasticity, Reynolds and load balance equations. The first two are partial differential equations requiring a finite element discretization of their corresponding field variables $\bar{U}$ and P, while the last one is an ordinary integral equation that is directly added to the system of equations along with the introduction of its corresponding field variable H_0 as an additional scalar unknown. In the following, the subscript *e* is assigned to the elastic part of the problem, *h* to the hydrodynamic part and *l* to the load balance part. Before detailing the MOR technique employed in the current work for the reduced FEM solution of transient EHL problems, it is first inevitable to develop the standard FEM modeling of the problem, from which the "reduced model" is derived. The associated model is referred as "full model".

3.1. Full Model

The weak form finite element formulation of the problem is obtained by multiplying each partial differential equation by its corresponding weight function (ψ_U and ψ_W for the linear elasticity equations and ψ_P for Reynolds equation) to get the corresponding weighted residual form. Then, each equation is integrated over its corresponding domain of application. Integration by parts is then applied, giving the below weak form formulation of the problem:

$$\begin{aligned}
&\text{Find } \left(\bar{U}, P, H_0\right) \text{ such that } \forall \left(\psi_U, \psi_W, \psi_P\right), \text{ one has:} \\
&\begin{cases}
\displaystyle\int_\Omega \left[\frac{\partial U}{\partial X}\frac{\partial \psi_U}{\partial X} + \frac{1}{2}\left(\frac{\partial U}{\partial Z} + \frac{\partial W}{\partial X}\right)\frac{\partial \psi_U}{\partial Z}\right] d\Omega = 0 \\
\displaystyle\int_\Omega \left[\frac{1}{2}\left(\frac{\partial U}{\partial Z} + \frac{\partial W}{\partial X}\right)\frac{\partial \psi_W}{\partial X} + \frac{\partial W}{\partial Z}\frac{\partial \psi_W}{\partial Z}\right] d\Omega + \int_{\Omega_c} \frac{P}{2}\psi_W \, d\Omega = 0 \\
\displaystyle\int_{\Omega_c} \left(\bar{\varepsilon}\frac{\partial P}{\partial X}\frac{\partial \psi_P}{\partial X} - \bar{\rho}H\frac{\partial \psi_P}{\partial X} + \frac{1}{\beta}\frac{\partial\left(\bar{\rho}H\right)}{\partial \bar{t}}\psi_P + \xi P\,\Theta\left(-P\right)\psi_P\right) d\Omega = 0 \\
\displaystyle\int_{\Omega_c} P \, d\Omega - \frac{\pi}{2} = 0
\end{cases}
\end{aligned} \tag{7}$$

Note that, out of simplicity, zero boundary integral terms have been omitted in the above weak form formulation. The only equation with a time-dependent term is Reynolds equation. As such, it requires a time-discretization of its transient term $\partial\left(\bar{\rho}H\right)/\partial\bar{t}$. Out of simplicity, throughout the remainder of this work, any term $\circ$ evaluated at the previous time step will be denoted $[\![\circ]\!]$. Thus, the transient term in Reynolds equation is time-discretized as follows, using a generalized-θ approximation:

$$\theta\frac{\partial\left(\bar{\rho}H\right)}{\partial\bar{t}} + \left(1-\theta\right)\left[\!\!\left[\frac{\partial\left(\bar{\rho}H\right)}{\partial\bar{t}}\right]\!\!\right] = \frac{\bar{\rho}H - [\![\bar{\rho}H]\!]}{\Delta\bar{t}} \tag{8}$$

In the above approximation, $\Delta\bar{t}$ corresponds to the time increment while θ is a parameter describing the time-discretization scheme. For $\theta = 0$, the first-order explicit forward Euler time-scheme is obtained, while for $\theta = 1/2$ and $\theta = 1$, the implicit second-order Crank-Nicolson and first-order backward Euler schemes are obtained. Generally, implicit time schemes are preferred over explicit ones for their unconditional stability. Multiplying each term of equation (8) by the weight function ψ_P and integrating over Ω_c, one gets:

$$\theta\int_{\Omega_c}\frac{\partial\left(\bar{\rho}H\right)}{\partial\bar{t}}\psi_P\, d\Omega + \left(1-\theta\right)\int_{\Omega_c}\left[\!\!\left[\frac{\partial\left(\bar{\rho}H\right)}{\partial\bar{t}}\psi_P\right]\!\!\right] d\Omega = \int_{\Omega_c}\frac{\bar{\rho}H - [\![\bar{\rho}H]\!]}{\Delta\bar{t}}\psi_P\, d\Omega \tag{9}$$

Then, from the weak form formulation of Reynolds equation, provided in equation (7), it can be noted that:

$$\int_{\Omega_c} \frac{\partial\left(\bar{\rho}H\right)}{\partial \bar{t}}\psi_P \, d\Omega = \int_{\Omega_c} \beta\left(-\bar{\varepsilon}\,\frac{\partial P}{\partial X}\frac{\partial \psi_P}{\partial X} + \bar{\rho}H\,\frac{\partial \psi_P}{\partial X} - \xi\, P\, \Theta(-P)\psi_P \right) d\Omega \tag{10}$$

Substituting equation (10) into (9), gives the time-discretized weak form formulation of Reynolds equation. Given that the linear elasticity and load balance equations do not include any time-dependent terms, the weak form formulation of the problem now reads:

Find $\left(\bar{U}, P, H_0\right)$ such that $\forall\left(\psi_U, \psi_W, \psi_P\right)$, one has:

$$\begin{cases}
\displaystyle\int_\Omega \left[\frac{\partial U}{\partial X}\frac{\partial \psi_U}{\partial X} + \frac{1}{2}\left(\frac{\partial U}{\partial Z} + \frac{\partial W}{\partial X}\right)\frac{\partial \psi_U}{\partial Z} \right] d\Omega = 0 \\
\displaystyle\int_\Omega \left[\frac{1}{2}\left(\frac{\partial U}{\partial Z} + \frac{\partial W}{\partial X}\right)\frac{\partial \psi_W}{\partial X} + \frac{\partial W}{\partial Z}\frac{\partial \psi_W}{\partial Z} \right] d\Omega + \int_{\Omega_c} \frac{P}{2}\psi_W \, d\Omega = 0 \\
\theta \displaystyle\int_{\Omega_c} \beta\left(\bar{\varepsilon}\,\frac{\partial P}{\partial X}\frac{\partial \psi_P}{\partial X} - \bar{\rho}H\,\frac{\partial \psi_P}{\partial X} + \xi\, P\, \Theta(-P)\psi_P \right) d\Omega \\
\quad + (1-\theta)\displaystyle\int_{\Omega_c} \left[\!\!\left[\beta\left(\bar{\varepsilon}\,\frac{\partial P}{\partial X}\frac{\partial \psi_P}{\partial X} - \bar{\rho}H\,\frac{\partial \psi_P}{\partial X} + \xi\, P\, \Theta(-P)\psi_P \right) \right]\!\!\right] d\Omega + \displaystyle\int_{\Omega_c} \frac{\bar{\rho}H - [\![\bar{\rho}H]\!]}{\Delta \bar{t}}\psi_P \, d\Omega \\
\quad \underbrace{\displaystyle\sum_{e=1}^{n_e^h} \int_{\Omega_{c,e}} \tau^e \left(H\,\frac{\partial \bar{\rho}}{\partial P}\frac{\partial \psi_P}{\partial X} \right) \left[\begin{array}{l} \theta\,\beta\left(-\dfrac{\partial}{\partial X}\left(\bar{\varepsilon}\,\dfrac{\partial P}{\partial X} \right) + \dfrac{\partial\left(\bar{\rho}H\right)}{\partial X} \right) \\ +(1-\theta)\left[\!\!\left[\beta\left(-\dfrac{\partial}{\partial X}\left(\bar{\varepsilon}\,\dfrac{\partial P}{\partial X} \right) + \dfrac{\partial\left(\bar{\rho}H\right)}{\partial X} \right) \right]\!\!\right] \\ + \dfrac{\bar{\rho}H - [\![\bar{\rho}H]\!]}{\Delta \bar{t}} \end{array} \right] d\Omega}_{SUPG\ term} = 0 \\
\displaystyle\int_{\Omega_c} P \, d\Omega - \frac{\pi}{2} = 0
\end{cases} \tag{11}$$

with: $\tau^e = \dfrac{h_e\left(\coth(Pe) - \dfrac{1}{Pe}\right)}{2\left|H\,\dfrac{\partial \bar{\rho}}{\partial P}\right| l_h}$ and $Pe = \dfrac{\left|H\,\dfrac{\partial \bar{\rho}}{\partial P}\right| h_e}{2\,\bar{\varepsilon}\, l_h}$

Note that, in the above formulation, a residual-based Streamline Upwind Petrov Galerkin (SUPG) [20] stabilizing term has been added, within Reynolds equation, to the interior of contact domain elements $\Omega_{c,e}$ ($e = 1 \cdots n_e^h$). This is because Habchi et al. [21] showed that Reynolds equation is of the convection-diffusion type and that it becomes convection-dominated under highly loaded conditions. As such, a standard Galerkin formulation would lead to spurious oscillations in the pressure distribution of highly loaded contacts. The use of stabilized FEM formulations (such as SUPG) is required to remedy these undesired purely numerical oscillations. In the definition of the SUPG term, h_e corresponds to the characteristic length of

element e, Pe is the local element Peclet number defining the ratio of convection to diffusion within the element and l_h corresponds to the element order used in approximating P. Finally, the fully-discretized FEM formulation of the problem is obtained by replacing the field variables $\bar{U}$ and P by their space-discretized equivalents. The latter are obtained from a standard finite element discretization, using Lagrange interpolation functions over their corresponding elements. Let n_n^e and n_n^h be the numbers of nodes within the 2D elastic domain Ω and 1D hydrodynamic domain Ω_c, respectively. Given that Reynolds equation is nonlinear, at every time step, the fully-discretized Galerkin formulation of the problem leads to an overall assembled matrix system, as a function of the increments of the nodal values of the field variables $\delta\bar{U}_i$ ($i=1\cdots n_n^e$), δP_i ($i=1\cdots n_n^h$) and δH_0, to be solved at every Newton iteration k, of the form:

$$\begin{bmatrix} [T_{ee}] & [T_{eh}] & \{0\} \\ [T_{he}] & [T_{hh}] & \{T_{hl}\} \\ \{0\} & \{T_{lh}\} & 0 \end{bmatrix}^{(k-1)} \begin{Bmatrix} \delta\bar{U}_1 \\ \vdots \\ \delta\bar{U}_{n_n^e} \\ \delta P_1 \\ \vdots \\ \delta P_{n_n^h} \\ \delta H_0 \end{Bmatrix}^{(k)} = -\begin{Bmatrix} \{0\} \\ \{R_h\} \\ R_l \end{Bmatrix}^{(k-1)} \tag{12}$$

The left-hand-side matrix in the above system is the Jacobian / tangent matrix, while the right-hand-side vector is the residual vector. The subscripts *e*, *h* and *l* are used to denote the elastic, hydrodynamic and load balance parts, respectively. For a detailed description of the composition of each sub-matrix and sub-vector within the above system of equations, the reader is referred to [5]. Note that the residual of the linear elasticity equations is nil, because they are linear and the initial guess will always be chosen to satisfy them. The total number of degrees of freedom (dofs) / unknowns n_{dof} of the full model is:

$$n_{dof} = 2\times n_n^e + n_n^h + 1 \tag{13}$$

This is because every node i of the 2D solid domain Ω is associated with two dofs (the nodal values of the dimensionless elastic displacement components U_i and W_i, in the x- and z-directions, respectively), while every node i of the 1D hydrodynamic domain Ω_c is associated with one dof (the nodal value P_i of the dimensionless pressure).

3.2. Reduced Model

The linear elasticity part of the "full model" described previously, solves for the elastic displacement field of the contacting solids over the entire 2D solid domain Ω. However, the solution of the EHL problem only requires knowledge of the normal component W of the elastic

displacement field within the 1D contact domain Ω_c, so that the geometry of the lubricating gap can be properly defined using the film thickness equation, provided in equation (4). Therefore, many linear elasticity dofs are being computed in vain. This brought Habchi and Issa [14] to develop the SCS technique to avoid solving for the unwanted dofs (the "slaves", denoted by the subscript *s*), while injecting their influence into the wanted / retained dofs (the "masters", denoted by the subscript *m*). The technique was originally developed for the steady-state EHL problem. In the current work, it is extended to the transient case. The subset of normal linear elasticity components $\hat{W}_i$ $(i=1\cdots n_n^h)$ over the 1D contact domain Ω_c are taken as the masters, while all other remaining linear elasticity dofs of the 2D solid domain Ω are taken as the slaves. Then, the linear elasticity part within equation (12): $[T_{ee}]\{\delta\bar{U}\}=-[T_{eh}]\{\delta P\}$, can be re-arranged as follows, by placing the slaves on top and the masters in the bottom:

$$\left[\begin{array}{c|c}[T_{ss}] & [T_{sm}]\\ \hline [T_{ms}] & [T_{mm}]\end{array}\right]\left\{\begin{array}{c}\{\delta U_s\}\\ \hline \{\delta U_m\}\end{array}\right\}=\left\{\begin{array}{c}\{\delta F_s\}\\ \hline \{\delta F_m\}\end{array}\right\} \qquad (14)$$

$$\text{with:}\quad \{\delta F\}=-[T_{eh}]\{\delta P\}\quad\text{and}\quad \{\delta U_m\}\equiv\{\delta\hat{W}\}$$

Then, the system of equations (14) can be expanded as follows:

$$\begin{aligned}[T_{ss}]\{\delta U_s\}+[T_{sm}]\{\delta\hat{W}\}&=\{\delta F_s\}\\ [T_{ms}]\{\delta U_s\}+[T_{mm}]\{\delta\hat{W}\}&=\{\delta F_m\}\end{aligned} \qquad (15)$$

From the first equation above: $\{\delta U_s\}=-[T_{ss}]^{-1}[T_{sm}]\{\delta\hat{W}\}+[T_{ss}]^{-1}\{\delta F_s\}$. Then, injecting this expression of $\{\delta U_s\}$ into the second equation of (15), a reduced system of equations is obtained as a function of the increments of the master dofs $\delta\hat{W}_i$ $(i=1\cdots n_n^h)$ only:

$$\begin{aligned}&[\hat{T}_{ee}]\{\delta\hat{W}\}=\{\delta\hat{F}\}\\ &\text{with:}\quad [\hat{T}_{ee}]=[T_{mm}]-[T_{ms}][T_{ss}]^{-1}[T_{sm}]\\ &\text{and}\quad \{\delta\hat{F}\}=\{\delta F_m\}-[T_{ms}][T_{ss}]^{-1}\{\delta F_s\}\end{aligned} \qquad (16)$$

Note that the above MOR technique is exact and introduces no additional errors to the solution scheme, since the influence of the slaves is not lost. It was injected into the masters, as can be seen in equation (16). Also note that the technique reduces by one the dimension of the linear elasticity part of the problem, confining it to the one-dimensional contact domain Ω_c. Then, at every time step, the reduced assembled system of equations to be solved at every Newton iteration k is obtained by replacing in equation (12) the full linear elasticity part by its equivalent reduced one, defined in equation (16):

$$\left[\begin{array}{c|c|c} \left[\hat{T}_{\mathrm{ee}}\right] & \left[\hat{T}_{\mathrm{eh}}\right] & \{0\} \\ \hline \left[\hat{T}_{\mathrm{he}}\right] & \left[T_{\mathrm{hh}}\right] & \{T_{\mathrm{hl}}\} \\ \hline \{0\} & \{T_{\mathrm{lh}}\} & 0 \end{array}\right]^{(k-1)} \left\{\begin{array}{c} \delta\hat{W}_1 \\ \vdots \\ \delta\hat{W}_{n_n^h} \\ \hline \delta P_1 \\ \vdots \\ \delta P_{n_n^h} \\ \hline \delta H_0 \end{array}\right\}^{(k)} = -\left\{\begin{array}{c} \{0\} \\ \hline \{R_{\mathrm{h}}\} \\ \hline R_{\mathrm{l}} \end{array}\right\}^{(k-1)} \tag{17}$$

Note that, since no external forces are applied to the slaves (according to the boundary conditions of equation (2), only a normal pressure force is applied to the contact domain nodes), then $\{\delta F_s\} = \{0\}$ and $\{\delta \hat{F}\} = \{\delta F_m\}$. This implies that, $\left[\hat{T}_{\mathrm{eh}}\right]$ is nothing but $\left[T_{\mathrm{eh}}\right]$, with the zero lines removed. Similarly, $\left[\hat{T}_{\mathrm{he}}\right]$ is nothing but $\left[T_{\mathrm{he}}\right]$, with the zero columns removed. This is because the hydrodynamic part of the problem is only connected to the elastic part through the masters. As such, the slaves make no contribution to either $\left[T_{\mathrm{eh}}\right]$ or $\left[T_{\mathrm{he}}\right]$. Their corresponding rows within $\left[T_{\mathrm{eh}}\right]$ and columns within $\left[T_{\mathrm{he}}\right]$ are empty.

Remark: In the evaluation of $\left[\hat{T}_{ee}\right]$ as defined in equation (16), in practice, the matrix $\left[T_{ss}\right]$ is never inverted as this would be computationally expensive. Instead, let $\left[T_{ss}\right]^{-1}\left[T_{sm}\right] = \left[\tilde{T}\right]$. Then, one can solve the system $\left[T_{ss}\right]\left[\tilde{T}\right] = \left[T_{sm}\right]$ for $\left[\tilde{T}\right]$. This resolution is much less computationally demanding, especially if a direct solver is used (e.g. LU decomposition). In fact, the computationally expensive part of factorizing $\left[T_{ss}\right]$ would only be done once and then, only the computationally inexpensive forward and backward substitutions would have to be repeated for every column of $\left[T_{sm}\right]$, to determine the corresponding column of $\left[\tilde{T}\right]$. Once $\left[\tilde{T}\right]$ is determined, according to equation (16), all that is left to do is to multiply it to the left by $\left[T_{ms}\right]$ and then substract the result from $\left[T_{mm}\right]$ to get $\left[\hat{T}_{ee}\right]$.

The total number of dofs $\hat{n}_{dof}$ of the reduced model is then:

$$\hat{n}_{dof} = 2 \times n_n^h + 1 \tag{18}$$

Given that $n_n^h \ll 2 \times n_n^e$ (since Ω_c is one-dimensional while Ω is two-dimensional), from a comparison of equations (13) and (18), it is clear that the size of the reduced model is significantly smaller than that of the full model. However, the downside is that $\left[\hat{T}_{\mathrm{ee}}\right]$ is dense,

leading to a semi-dense tangent matrix, in equation (17). In [14], it was shown that the solution of the semi-dense reduced matrix system would be more computationally expensive than that of the sparse full matrix system, unless a splitting procedure is applied. It consists in splitting $\left[\hat{T}_{\text{ee}}\right]$ into "near" and "far" contributions $\left[\hat{T}_{ee}^{n}\right]$ and $\left[\hat{T}_{ee}^{f}\right]$, respectively, such that: $\left[\hat{T}_{\text{ee}}\right]=\left[\hat{T}_{ee}^{n}\right]+\left[\hat{T}_{ee}^{f}\right]$. For each node of the contact domain Ω_c, and thus for each corresponding row within $\left[\hat{T}_{\text{ee}}\right]$, the near contributions are those of nodes belonging to the same element(s) (i.e. nodes that are connected to it in a finite element sense). All remaining contributions are moved toward $\left[\hat{T}_{ee}^{f}\right]$. Incorporating the splitting procedure into the system of equations (17), it becomes:

$$\begin{bmatrix} \left[\hat{T}_{ee}^{n}\right] & \left[\hat{T}_{\text{eh}}\right] & \{0\} \\ \left[\hat{T}_{\text{he}}\right] & \left[T_{\text{hh}}\right] & \{T_{\text{hl}}\} \\ \{0\} & \{T_{\text{lh}}\} & 0 \end{bmatrix}^{(k-1)} \begin{Bmatrix} \{\delta\hat{W}\}^{(i)} \\ \{\delta P\}^{(i)} \\ \delta H_0{}^{(i)} \end{Bmatrix}^{(k)} = -\begin{Bmatrix} \left[\hat{T}_{ee}^{f}\right]\{\delta\hat{W}\}^{(i-1)} \\ \{R_{\text{h}}\} \\ R_{\text{l}} \end{Bmatrix}^{(k-1)} \tag{19}$$

Note that the splitting procedure allows retrieving a standard 1D-1D sparsity pattern, since the sparsity patterns of $\left[\hat{T}_{ee}^{n}\right]$ and $\left[T_{\text{hh}}\right]$ are identical. At every time step, the resolution of the system of equations (19) entails two embedded iterative procedures. The first one is the overall nonlinear iterative resolution procedure, denoted by the iteration index k. The second one is embedded within each iteration k of the nonlinear resolution procedure and it consists in applying splitting corrections / iterations, denoted by the iteration index i. The overall numerical procedure is described next.

Remark: Note that, without the splitting procedure, the number of operations required for factorizing the Jacobian matrix of the reduced model would actually be increased with respect to that of the full model. This number is governed by the number of nonzero entries within the Jacobian matrix. The latter only differs for the submatrix $\left[T_{ee}\right]$, between the full and reduced models. In fact, remember that $\left[T_{hh}\right]$, $\{T_{\text{hl}}\}$ and $\{T_{\text{lh}}\}$ are unaltered by the model reduction procedure, while $\left[\hat{T}_{\text{eh}}\right]$ and $\left[\hat{T}_{\text{he}}\right]$ are deduced from their full model counterparts $\left[T_{\text{eh}}\right]$ and $\left[T_{\text{he}}\right]$ by a simple removal of zero rows and columns, respectively. For the mesh employed in the current work (see section 4) for instance, the number of nonzero entries of $\left[T_{ee}\right]$ is 357,108. Without splitting, the

number of nonzero entries of the dense matrix $\left[\hat{T}_{\text{ee}}\right]$ is increased to 826,281, leading to a significant increase in the number of operations required for factorizing the Jacobian matrix. It is only when splitting is applied that this number of operations decreases, since the number of nonzero entries is reduced to 3,633 within $\left[\hat{T}_{ee}^{n}\right]$. This leads to significant speedups in computational times, as will be discussed in section 4.

3.3. Overall Numerical Procedure

The overall numerical procedure consists of a recursive time-stepping algorithm. The first step consists in defining an initial guess for the recursive procedure. The initial guess is dictated by the initial conditions of the problem and will not be detailed at this stage, as it is problem-specific. Starting with the defined initial guess, at each of the following time steps, a solution is sought, while using the previous time step solution as initial guess. This procedure is repeated until the entire time domain is covered.

At every time step, the problem is formulated as a function of the current as well as the previous time step variables, as detailed in section 3.1. The problem formulation leads to the reduced system of equations (19), which is solved for the current time step variables $\left\{\hat{W}\right\}$, $\{P\}$ and H_0. These are obtained from an iterative nonlinear procedure, consisting of a repeated resolution of the system of equations (19) at every iteration k, until convergence is attained. The overall assembled matrix system (19) is solved using a direct solver based on a multi-frontal sparse LU decomposition method: UMFPACK [22]. Given the highly nonlinear nature of Reynolds equation, a damped-Newton procedure [23] is used for the nonlinear resolution process. It consists in adding at every iteration k, a fraction of the solution increment, to the solution obtained at the previous iteration $k-1$ (rather than the full increment, as done with the standard Newton method). For this, an optimal fraction is computed at every iteration k to minimize error, while maintaining the updated solution within the relatively narrow convergence radius of Newton methods. Algorithmic details and convergence criteria of the damped-Newton method can be found in [5].

Within every iteration k of the damped-Newton procedure, due to splitting, another iterative procedure is embedded, denoted by the iteration index i. In fact, at every splitting iteration i, the far contribution of the elastic problem is evaluated on the right-hand-side using $\left\{\delta\hat{W}\right\}^{(i-1)}$, obtained at the previous iteration $i-1$. Then, the system of equations (19) is solved repeatedly to get updated values of $\left\{\delta\hat{W}\right\}^{(i)}$, $\{\delta P\}^{(i)}$ and $\delta H_0^{(i)}$, until convergence is attained. That is, until the normalized *L2*-norm of the absolute difference between increment vectors of the overall solution $\left\{\left\{\delta\hat{W}\right\},\{\delta P\},\delta H_0\right\}$, between two consecutive splitting iterations, falls below 10^{-4}. Note that the tangent matrix and the residuals of the hydrodynamic and load balance problems ($\left\{R_h\right\}$ and R_l,

respectively) are not re-evaluated at every splitting iteration i. These are only re-evaluated at every Newton iteration k. This being said, since the tangent matrix is the same for every splitting iteration i, the repeated resolution of the system of equations (19) at every iteration i is a relatively computationally inexpensive operation, since the LU factorization is not repeated and only the forward and backward substitution operations are carried out, while updating the right-hand-side, specifically the elastic part.

Remark 1: At every Newton iteration k, the initial guess for $\left\{\delta\hat{W}\right\}$ for the splitting procedure is taken as: $\left\{\delta\hat{W}\right\}^{(0)} = \{0\}$. That is, for the first splitting iteration ($i=1$) of every Newton iteration k, the right-hand-side sub-vector of the linear elasticity part is nil.

Remark 2: Since the linear elasticity and load balance equations are linear and time-independent, the sub-matrices $\left[\hat{T}_{\text{ee}}\right]$ ($\left[\hat{T}^{n}_{ee}\right]$ and $\left[\hat{T}^{f}_{ee}\right]$) and $\left[\hat{T}_{\text{eh}}\right]$, as well as the sub-vector $\{T_{\text{lh}}\}$ only need to be evaluated once. Their values are then kept the same at all time steps, for all iterations k of the nonlinear resolution procedure and all iterations i of the splitting procedure. Besides, for a given mesh, the evaluation of $\left[\hat{T}_{\text{ee}}\right]$ can be done once and then stored for later use. This is because the sub-matrix $\left[T_{\text{ee}}\right]$ from which it originates, only depends on the employed mesh. It is independent of the operating conditions. It was also made independent of the solid material properties, through the choice of equivalent properties discussed in section 2.

4. Results and Discussion

In this section, some typical transient isothermal Newtonian line contact simulations are carried out to reveal the effectiveness of the proposed MOR technique in reducing the size of the corresponding FEM models, as well as the associated computational times. All numerical tests are carried out using a single Intel Core i7 2.7 GHz processor. The employed mesh throughout this section is shown in figure 3. It corresponds to the "*Fine*" mesh case employed in [14], which was shown to provide grid-independent solutions. The mesh consists of $n_e^e = 5{,}132$ triangular elements used in discretizing the 2D solid domain Ω of the elastic part. The projection of this mesh over the 1D contact domain Ω_c is used as the mesh of the hydrodynamic part, avoiding any unnecessary interpolation between their associated field variables. The 1D mesh of the hydrodynamic part consists of $n_e^h = 454$ line elements. Lagrange quadratic shape functions are used in approximating U, W and P. Thus, 6-node triangular elements are used in approximating U and W, while 3-node line elements are used in approximating P. The total number of nodes within the 2D solid domain Ω is: $n_n^e = 10{,}773$, while that of the 1D contact domain Ω_c is: $n_n^h = 909$. This being said, the total numbers of degrees of freedom of the full and reduced models are: $n_{dof} = 22{,}456$ and $\hat{n}_{dof} = 1{,}819$, respectively. Note that the employed mesh

has been specifically designed to meet the specificities of the EHL problem. That is, the mesh size is relatively small in the vicinity of the contact domain (where a high solution precision is required) and then increases gradually with distance from the contact.

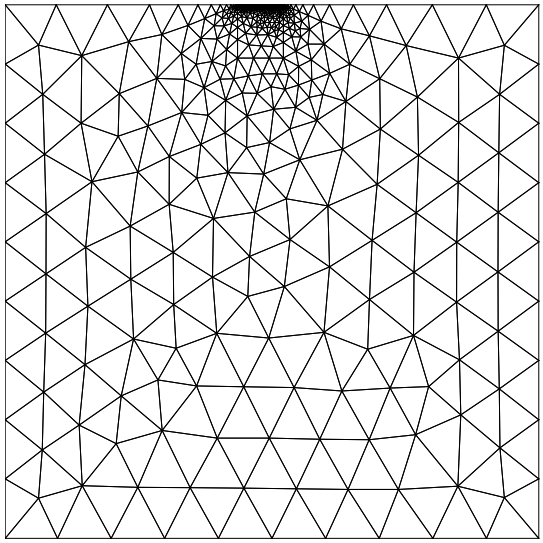

Figure 3: Employed mesh for the transient EHL line contact test cases

Two test cases are considered in the following: the first one corresponds to the passage of a surface indent through the contact, while the second corresponds to a sudden deceleration in contact mean entrainment speed u_m. For both test cases, steel-steel contacts are considered ($E_1 = E_2 = 210$ GPa and $\upsilon_1 = \upsilon_2 = 0.3$) under pure-rolling conditions ($u_1 = u_2$), with a cylinder radius $R = 15$ mm. As for the lubricant properties, the values $\mu_0 = 10$ mPa·s and $\alpha = 20$ GPa^{-1} are adopted. A constant time-stepping strategy is adopted for all test cases with $\Delta\bar{t} = 0.01$ and a Crank-Nicolson time-discretization scheme ($\theta = 1/2$) is used. The penalty term for all simulations is defined as: $\xi = \xi_0 h_e$, with $\xi_0 = 10^6$ [5].

4.1. Passage of a Surface Indent through the Contact

First, the case of the passage of a surface indent through the contact is considered under pure-rolling conditions, with a mean entrainment speed $u_m = 1 m/s$ and an external applied load per unit length $F = 2$ MN/m ($p_h = 2.2$ GPa). The indent is placed on one of the contacting surfaces, by defining the surface feature term $\bar{S}(X, \bar{t})$ in equation (4) as follows:

$$\bar{S}(X, \bar{t}) = A_f \; 10^{-10\left(\frac{X - X_f}{\omega_f}\right)^2} \cos\left(2\pi \frac{X - X_f}{\omega_f}\right) \qquad \text{with:} \quad X_f = X_s + \bar{t} \tag{20}$$

The geometry of the employed indent is shown in figure 4. The parameter A_f represents its dimensionless amplitude, while ω_f corresponds to its dimensionless wavelength and X_f

corresponds to the dimensionless location of its center within the contact. From the definition of X_f provided in equation (20), it results that X_s is nothing else but the dimensionless location of the indent center at $\bar{t} = 0$. Values of $A_f = 0.01$, $\omega_f = 1$ and $X_s = -5$ are chosen here. For the current test case, the dimensionless time is defined as $\bar{t} = t\,u_m / a_h$, which results in a time non-dimensionalization parameter $\beta = 1$, within Reynolds equation. For more details on the non-dimensional write-up of the different EHL equations, the reader is referred to [5]. Note that the term a_h / u_m appearing in the definition of $\bar{t}$ simply corresponds to the time it takes for the indent to travel a distance that is equivalent to the contact half-width a_h (or a non-dimensional travel distance of unity). The time domain is chosen such that the surface feature completely traverses the contact from left to right, with $t_0 = 0$ and $\tilde{t} = 6.5$. At the beginning of the simulation ($\bar{t} = 0$), the indent is completely outside the contact domain. This way, the initial guess is taken as the steady-state solution of the equivalent smooth case, operating under the same conditions. This assumes that the contact was operating in steady-state regime before the feature reached it. The dimensionless pressure and film thickness profiles of the smooth steady-state solution are shown in figure 5. These are obtained using the steady-state reduced FEM model developed in [14].

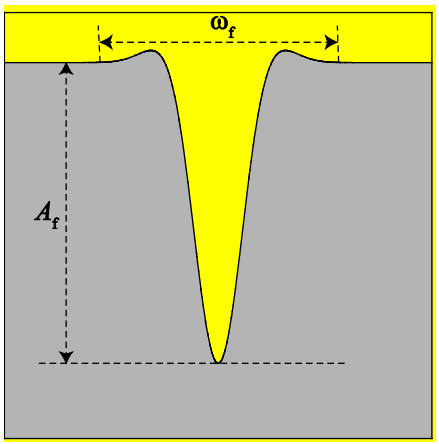

Figure 4: Geometry of the indent, placed on one of the contacting surfaces

As long as the indent does not approach the flat central area of the contact, disruptions to the dimensionless pressure and film thickness profiles are barely noticeable and these remain virtually the same as the smooth steady-state profiles shown in figure 5 (except for the presence of the unaltered indent within the film thickness profile). However, when the indent approaches the central zone, it starts having a much more significant influence on both pressure and film thickness distributions. The results obtained using both the full and reduced models are shown in figure 6 for the passage of the indent through the contact at different dimensionless times ($\bar{t} = 4$, 4.5, 5 and 5.5), corresponding to different positions within the contact of the indent center ($X_f = -1$, -0.5, 0 and 0.5). Clearly, as the indent enters the central flat zone of the contact, it leads to a localized disruption (in its vicinity) of both the pressure and film thickness profiles.

Given that the presence of the indent locally increases film thickness in its vicinity, a localized pressure decrease is observed in that region. These observations are in agreement with similar tests reported in the literature [24]. Note that the results shown in figure 6 reveal a perfect agreement between the full and reduced model solutions. This is not surprising, given that the employed SCS technique is exact and as such, it introduces no additional errors to the solution with respect to the full model. In terms of performance though, the computational times are 1122s with the full model and 75s with the reduced model. Thus, a speed-up in computational time of the order of 15:1 is achieved by the proposed MOR technique, without any compromise on the accuracy of the solution. At every time step, only a few Newton iterations are needed for convergence of the nonlinear resolution procedure. This is due to two factors: first, the fast convergence characteristics associated with full-coupling and Newton methods and second, the use of the previous time step solution as initial guess, at every time step. Also, very few splitting iterations are needed (generally, less than 10) at every Newton iteration. For more details on the performance characteristics of the employed damped-Newton method and the splitting procedure, the interested reader is referred to [14].

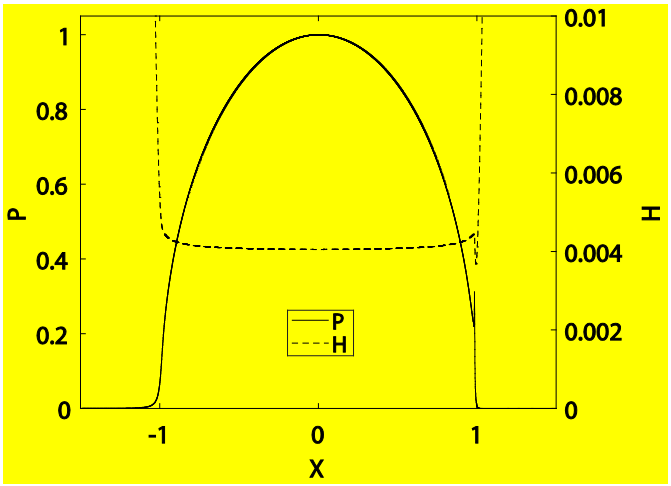

Figure 5: Smooth steady-state dimensionless pressure and film thickness distributions (before the indent enters the contact domain)

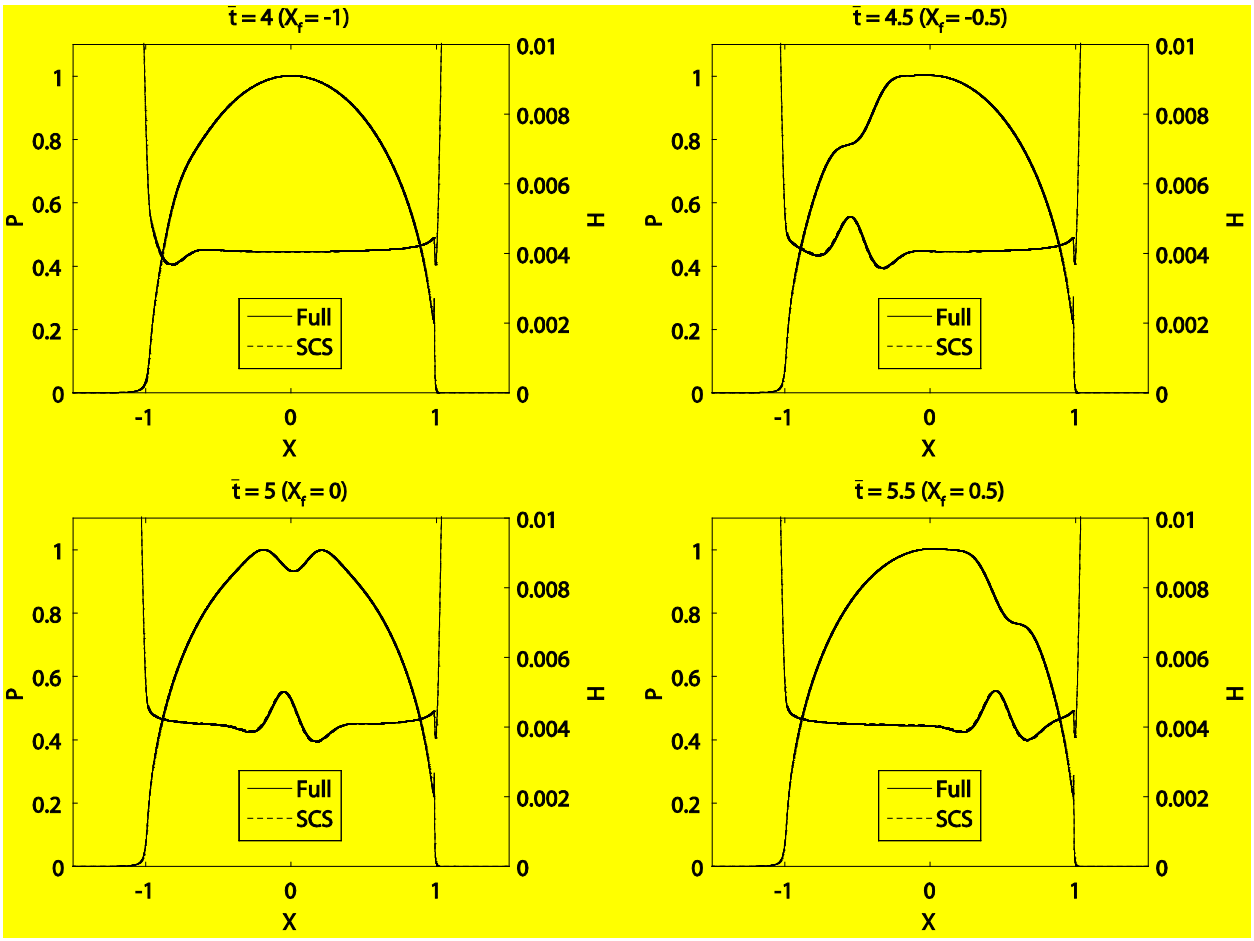

Figure 6: Dimensionless pressure and film thickness distributions at different dimensionless times $\bar{t}$, during the passage of the indent through the contact, obtained using the full and reduced models

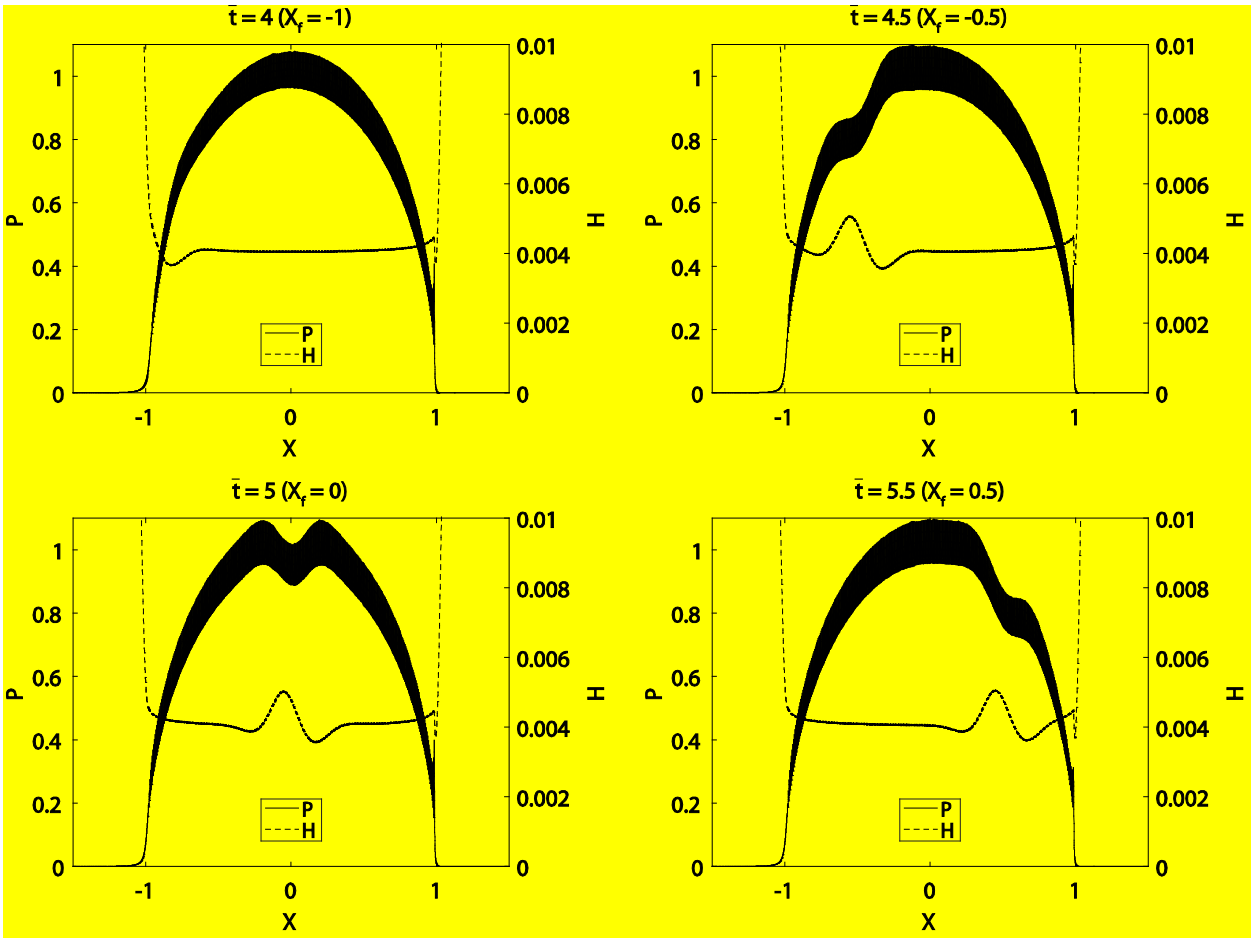

Figure 7: Dimensionless pressure and film thickness distributions at different dimensionless times $\bar{t}$, during the passage of the indent through the contact, obtained using the reduced model (without SUPG)

Finally, note that for this test case, which corresponds to a relatively heavy loaded contact ($p_h = 2.2$ GPa), the use of the SUPG stabilized formulation is mandatory. Without it, the dimensionless pressure and film thickness profiles would exhibit spurious oscillations, as shown in figure 7. In fact, figure 7 shows the same results for the passage of the surface indent through the contact, obtained using the reduced model, but without the addition of the SUPG stabilizing term, as provided in equation (11). This results in spurious oscillations in the solution. The amplitude of the oscillations is more pronounced though for pressure than they are for film thickness. This is not surprising as any oscillations in film thickness are expected to have an amplified influence on pressure, because film thickness appears to the cubic power within Reynolds equation (see equation (3)).

4.2. Sudden Deceleration

In the current section, a smooth contact is considered, subject to a sudden deceleration in contact mean entrainment speed u_m, under pure-rolling conditions with an external applied load per unit length $F = 0.2$ MN/m ($p_h = 0.7$ GPa). For this, the contact is assumed to be operating

steadily, at an initial mean entrainment speed $u_{m,i}$, before it is subjected to a sudden constant deceleration to a final mean entrainment speed $u_{m,f} \ll u_{m,i}$, during a period of time t_d. Therefore, a linear (in time) mean entrainment speed profile is obtained, whereby u_m is reduced from $u_{m,i}$ to $u_{m,f}$, within a period of time t_d. This is achieved by defining u_m as a function of dimensionless time $\bar{t}$ as follows:

$$u_m\left(\bar{t}\right) = u_{m,i} + \bar{t}\left(u_{m,f} - u_{m,i}\right) \tag{21}$$

with $\bar{t}$ being defined in this case as $\bar{t} = t/t_d$. This results in a time non-dimensionalization parameter $\beta = u_m t_d / a_h$, within Reynolds equation. For more details on the non-dimensional write-up of the different EHL equations, the reader is referred to [5]. The time domain is chosen such that the entire deceleration phase is covered, with $t_0 = 0$ and $\tilde{t} = 1$. The values of $u_{m,i} = 1 m/s$, $u_{m,f} = 0.02 m/s$ and $t_d = 1 s$ are adopted for the current test case. The initial guess is taken as the steady-state solution for $u_m = u_{m,i}$, since the contact was assumed to operate under steady-state regime before it was subjected to the sudden deceleration.

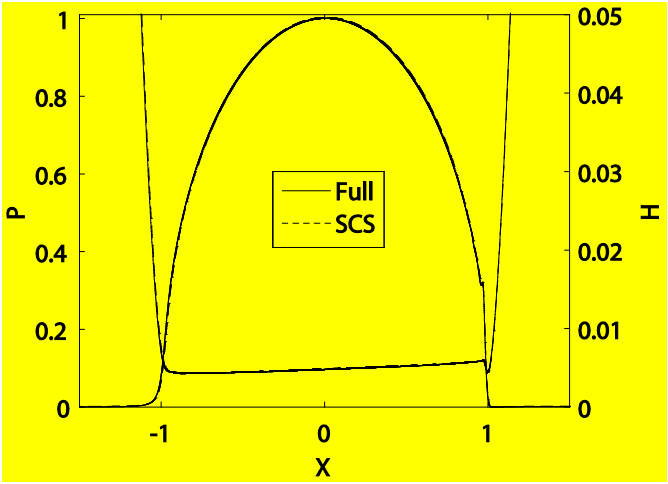

Figure 8: Dimensionless pressure and film thickness distributions at the end of the deceleration phase ($\bar{t} = 1$), obtained using the full and reduced models

The dimensionless pressure and film thickness distributions at the end of the deceleration phase ($\bar{t} = 1$), obtained using both the full and reduced models are shown in figure 8. Because of the sudden deceleration of the contact surfaces, film thickness generally experiences a sudden drop. However, the drop is faster on the inlet side of the contact compared to the outlet. This could not have been observed with a steady-state analysis (with $u_m = u_{m,f}$), which would have predicted a quasi-flat film thickness profile in the central contact zone. These observations are in agreement with similar tests reported in the literature, both experimentally [25] and numerically [26]. Note that the results shown in figure 8 also reveal a perfect agreement between the full and reduced model solutions. In terms of performance though, the computational times are 74s with

the full model and 5s with the reduced model. Thus, a speed-up in computational time of the order of 15:1 is achieved by the proposed MOR technique, without any compromise on the accuracy of the solution. Similar to the indent test case, at every time step, only a few Newton iterations are needed for convergence of the nonlinear resolution procedure. Also, very few splitting iterations are needed (generally, less than 10) at every Newton iteration. For more details on the performance characteristics of the employed damped-Newton method and the splitting procedure, the interested reader is referred to [14].

Remark: The mesh employed in this section was shown in [14] to be of "just enough" finesse to guarantee grid-independent solutions. For the applications considered in this section, there is no point in refining this mesh as this would not result in any significant improvement in accuracy. But should a more demanding application be considered (e.g. real surface roughness), which requires much higher mesh densities, the speed-up in computational time between the full and reduced models would be expected to increase. This is because the reduction order generally increases when the mesh density is increased (or the mesh size is reduced) [14].

5. Conclusion

The current work presents an extension of the reduced finite element modeling framework proposed in [14] for the solution of steady-state EHL problems, to account for transient effects. The MOR technique consists in applying a Schur-complement method to the linear elasticity part within EHL problems. As such, it is exact and introduces no additional errors with respect to the standard finite element solution. However, it gives rise to a semi-dense Jacobian matrix. This is why it is complemented with a splitting procedure, allowing it to retrieve a standard finite-element-like sparsity pattern for the Jacobian matrix. The proposed model was used to run two typical transient EHL simulations: the passage of a surface indent through the contact and a sudden deceleration in contact mean entrainment speed. The results revealed a perfect agreement between the pressure and film thickness distributions obtained from the full and reduced models, except that the latter offered a speed-up in computational times of the order of 15:1 with respect to the former. Finally, note that out of simplicity, the proposed modeling framework was applied to the case of isothermal Newtonian line contacts only. However, the approach may be easily extended to more complex configurations e.g. point contacts with the inclusion of thermal and non-Newtonian effects.

Nomenclature

α	: Lubricant pressure-viscosity coefficient (Pa^{-1})
β	: Time non-dimensionalization parameter
$\Delta\bar{t}$	: Dimensionless time increment
μ_0	: Lubricant viscosity at ambient pressure (Pa.s)
$\bar{\mu}$	: Dimensionless lubricant viscosity

υ : Equivalent Poisson coefficient

υ_1 : Plane Poisson coefficient

υ_2 : Cylinder Poisson coefficient

Ω : Two-dimensional solid domain

Ω_c : One-dimensional contact domain

Θ : Heaviside function

ω_f : Surface feature dimensionless wavelength

ρ : Lubricant density (kg/m^3)

$\overline{\rho}$: Dimensionless lubricant density

ρ_0 : Lubricant density at ambient pressure (kg/m^3)

σ_n : Normal stress tensor component (Pa)

σ_t : Tangential stress tensor component (Pa)

ξ : Penalty term parameter

ξ_0 : Penalty term constant parameter

ψ_U, ψ_W : Finite element trial functions for the elastic problem

ψ_P : Finite element trial function for the hydrodynamic problem

a_h : Hertzian contact half-width (m)

A_f : Surface feature dimensionless amplitude

E : Equivalent Young's modulus (Pa)

E_1 : Plane Young's modulus of elasticity (Pa)

E_2 : Cylinder Young's modulus of elasticity (Pa)

F : Contact external applied load per unit length (N/m)

h : Lubricant film thickness (m)

h_e : Element characteristic length

H : Dimensionless lubricant film thickness

H_0 : Film thickness constant parameter

l_h : Interpolation order for hydrodynamic part elements

n_e^h : Number of elements in the 1D hydrodynamic domain

n_e^e : Number of elements in the 2D elastic domain

n_n^h : Number of nodes in the 1D hydrodynamic domain

n_n^e : Number of nodes in the 2D elastic domain

n_{dof} : Total number of degrees of freedom of the full EHL model

$\hat{n}_{dof}$: Total number of degrees of freedom of the reduced EHL model

p : Pressure (Pa)

P : Dimensionless pressure

P_0 : Dimensionless pressure initial guess

Pe : Local element Peclet number

p_h : Hertzian contact pressure (Pa)

R : Cylinder radius (m)

$\overline{S}$: Fim thickness equation dimensionless surface feature term

t : Time (s)

t_d : Deceleration time (s)

$\overline{t}$: Dimensionless time

t_0 : Initial dimensionless time

$\tilde{t}$: Final dimensionless time

$u,\ w$: x and z-components of the solid elastic displacement field (m)

$U,\ W$: Dimensionless x and z-components of the solid elastic displacement field

u_1 : Plane surface velocity (m/s)

u_2 : Cylinder surface velocity (m/s)

u_m : Contact mean entrainment speed (m/s)

$u_{m,i}$: Initial contact mean entrainment speed (m/s)

$u_{m,f}$: Final contact mean entrainment speed (m/s)

$x,\ y,\ z$: Space coordinates (m)

$X,\ Z$: Dimensionless space coordinates

X_f : Dimensionless position of surface feature center

X_s : Initial dimensionless position of surface feature center

Subscripts

1 : Flat plane

2 : Cylinder

e : Elastic

h : Hydrodynamic

l : Load balance

m : Masters

s : Slaves

Dimensionless Parameters

$$X=\frac{x}{a_h} \quad Z=\frac{z}{a_h} \quad H=\frac{hR}{a_h^2} \quad U=\frac{uR}{a_h^2} \quad W=\frac{wR}{a_h^2}$$

$$P=\frac{p}{p_h} \quad \overline{\rho}=\frac{\rho}{\rho_0} \quad \overline{\mu}=\frac{\mu}{\mu_0} \quad \overline{t}=\begin{cases} t\,u_m/a_h & \text{(overrolling of an indent)} \\ t/t_d & \text{(sudden deceleration)} \end{cases}$$

References

[1] Venner C. H. and Lubrecht A. A. – Multilevel Methods in Lubrication, Elsevier, 2000.

[2] Reynolds O. – On the Theory of the Lubrication and its Application to Mr. Beauchamp Tower's Experiments, Including an Experimental Determination of the Viscosity of Olive Oil, *Philiosophical Transactions of the Royal Society*, 1886, vol. 177, pp. 157-234.

[3] Love A. E. H. – Mathematical Theory of Elasticity, Dover, New York, 1994.

[4] Habchi W., Eyheramendy D., Vergne P. and Morales-Espejel G. E. – A Full-System Approach of the Elastohydrodynamic Line/Point Contact Problem, *ASME Journal of Tribology*, 2008, vol. 130, 021501.

[5] Habchi W. - Finite Element Modeling of Elastohydrodynamic Lubrication Problems, 2018, *Wiley*, Chichester, UK.

[6] Paulson N. R., Sadeghi F. and Habchi W. - A Coupled Finite Element EHL and Continuum Damage Mechanics Model for Rolling Contact Fatigue, *Tribology International*, 2017, vol. 107, pp. 173-183.

[7] Qu Z.Q. – Model Order Reduction Techniques with Applications in Finite Element Analysis, Springer, UK, 2004.

[8] Habchi W. and Issa J. – Fast and Reduced Full-System Finite Element Solution of EHL Problems: Line Contacts, *Advances in Engineering Software*, 2013, vol. 56, pp. 51-62.

[9] Habchi W. - Reduced Order Finite Element Model for Elastohydrodynamic Lubrication: Circular Contacts, *Tribology International*, 2014, vol. 71, pp. 98-108.

[10] Krinner A. and Rixen D. J. – Interface Reduction Methods for Mechanical Systems with Elastohydrodynamic Lubricated Revolute Joints, *Multibody System Dynamics*, 2018, vol. 42, pp. 79-96.

[11] Bampton M. C. and Craig R. R. – Coupling of Substructures for Dynamic Analyses, *AIAA Journal*, 1968, vol. 6 (7), pp. 1313-1319.

[12] Maier D., Hager C., Hetzler H., Fillot N., Vergne P., Dureisseix D. and Seemann W. – A Nonlinear Model Order Reduction Approach to the Elastohydrodynamic Problem, *Tribology International*, 2015, vol. 82, pp. 484–492.

[13] Maier D., Hager C., Hetzler H., Fillot N., Vergne P., Dureisseix D. and Seemann W. – Fast Solution of Transient Elastohydrodynamic Line Contact Problems using the Trajectory Piecewise Linear Approach, *ASME Journal of Tribology*, 2016, vol. 138, 011502.

[14] Habchi W. and Issa J. S. - An Exact and General Model Order Reduction Technique for the Finite Element Solution of Elastohydrodynamic Lubrication Problems, *ASME Journal of Tribology*, 2017, vol. 139 (5), 051501.

[15] Guyan R. J. – Reduction of Stiffness and Mass Matrices, *AIAA Journal*, 1965, vol. 3(2), p. 380.
[16] Hertz H. – Uber die Berührung fester Elastischer Körper, *Journal für die reine und angewandte Mathematik*, 1881, vol. 92, pp. 156–171.
[17] Raisin J., Fillot N., Dureisseix D., Vergne P. and Lacour V. – Characteristic Times in Transient Thermal Elastohydrodynamic Line Contacts, *Tribology International*, 2015, vol. 82, pp. 472-483.
[18] Dowson D. and Higginson G. R. – Elastohydrodynamic Lubrication, *Pergammon*, Oxford, 1977.
[19] Roelands C. J. A. - Correlational Aspects of the Viscosity-Temperature-Pressure Relationship of Lubricating Oils, *PhD Thesis*, Technische Hogeschool Delft, The Netherlands, 1966.
[20] Brooks A. N. and Hughes T. J. R. - Streamline-Upwind/Petrov-Galerkin Formulations for Convective Dominated Flows with Particular Emphasis on the Incompressible Navier-Stokes Equations. *Comp. Meth. Appl. Mech. Engnrg.*, 1982, vol. 32, pp.199-259.
[21] Habchi W., Eyheramendy D., Vergne P. and Morales-Espejel G. E. – Stabilized Fully-Coupled Finite Elements for Elastohydrodynamic Lubrication Problems, *Advances in Engineering Software*, 2012, vol. 46, pp. 4-18.
[22] Davis T. A. and Duff I. S. - An Unsymmetric-Pattern Multifrontal Method for Sparse LU Factorization, *SIAM Journal on Matrix Analysis and Applications*, 1997, vol. 18, no. 1, pp. 140-158.
[23] Deuflhard P. – Newton Methods for Nonlinear Problems, Affine Invariance and Adaptive Algorithms. *Springer*, Germany, 2004.
[24] Venner C. H. – Multilevel Solution of the EHL Line and Point Contact Problems, *PhD Thesis*, University of Twente, Enschede, The Netherlands, 1991.
[25] Sugimura J., Jones W. R. and Spikes H. A. – EHD Film Thickness in non-Steady State Contacts, *ASME Journal of Tribology*, 1998, vol. 120(3), pp. 442-452.
[26] Al Samieh M. and Rahnejat H. – Ultra-Thin Lubricating Films under Transient Conditions, *Journal of Physics D – Applied Physics*, 2001, vol. 34(17), pp. 2610-2621.